

High Performance and Cost-Effective Direct Methanol Fuel Cells: Fe-N-C Methanol-Tolerant Oxygen Reduction Reaction Catalysts

David Sebastián,^[a] Alexey Serov,^[b] Kateryna Artyushkova,^[b] Jonathan Gordon,^[b] Plamen Atanassov,^{*,[b]} Antonino S. Aricò,^[a] and Vincenzo Baglio^{*,[a]}

Direct methanol fuel cells (DMFCs) offer great advantages for the supply of power with high efficiency and large energy density. The search for a cost-effective, active, stable and methanol-tolerant catalyst for the oxygen reduction reaction (ORR) is still a great challenge. In this work, platinum group metal-free (PGM-free) catalysts based on Fe-N-C are investigated in acidic medium. Post-treatment of the catalyst improves the ORR activity compared with previously published PGM-free formulations and shows an excellent tolerance to the presence of methanol. The feasibility for application in DMFC under a wide

range of operating conditions is demonstrated, with a maximum power density of approximately 50 mW cm⁻² and a negligible methanol crossover effect on the performance. A review of the most recent PGM-free cathode formulations for DMFC indicates that this formulation leads to the highest performance at a low membrane-electrode assembly (MEA) cost. Moreover, a 100 h durability test in DMFC shows suitable applicability, with a similar performance-time behavior compared to common MEAs based on Pt cathodes.

Introduction

Growing energy demand and environmental concerns have driven the search for new technologies to produce green energy because fossil fuels are a finite resource and their direct combustion raises pollution levels.^[1] Fuel cells are a competitive alternative for the supply of energy with high efficiency and low emission levels by conversion of chemical energy into electricity through electrochemical reactions. The fuel cell configuration (i.e., fuel, electrolyte, start-up/shut-down speed) used for a particular application depends on the purpose and limitation of the operating temperature.^[2]

Direct alcohol fuel cells, in particular direct methanol fuel cells (DMFCs), are considered a key enabling technology for powering portable devices in a sustainable economy based on highly efficient and renewable sources.^[3-5] DMFCs are very convenient for prolonged duration systems owing to the high energy content of methanol (6100 mWh g⁻¹).^[5] The remaining technical barrier that needs to be overcome for the develop-

ment of DMFCs is their low power density resulting from the sluggish kinetics of the methanol oxidation reaction (MOR) and oxygen reduction reaction (ORR). The most critical factors are the high cost of the anode and cathode catalysts, which are usually based on expensive and scarce platinum metal, and the crossover effect, that is, the permeation of the alcohol through the polymeric membrane, which creates a mixed potential at the cathode and decreases the overall efficiency.^[6-9] Although Pt presents the highest activity for the ORR, it is also a good methanol dehydrogenation/oxidation catalyst, which implies that if methanol and oxygen are present the selectivity toward ORR is far lower than 100%.

The high cost of the cathode and the detrimental effect of methanol crossover can be greatly reduced with a single solution: the use of platinum group metal (PGM)-free catalysts in the cathode side. These are characterized by a much lower cost than Pt^[10-12] and by an extraordinarily high selectivity towards the oxygen reduction (neither significant methanol poisoning nor oxidation). Many non-platinum formulations have shown great activity compared to platinum catalysts, but the performance, durability and stability are still very low in a single cell.^[13,14] Until now, M-N-C catalysts (M=transition metal such as Fe or Co) have shown great promise owing to their good ORR activity and have been targeted for low cost hydrogen-fuel cells.^[15,16] The research interest for their application in DMFCs has arisen recently. Investigations that have reported DMFCs can be divided into the following categories: Fe-based catalysts mostly in acidic DMFCs^[17-23] as well as a few in alkaline type DMFCs,^[22,24,25] and Co-based catalysts in acidic^[19,26,27] or alkaline DMFCs.^[28] Other PGM-free formulations, mainly chemically or physically modified carbon^[29-34] or other

[a] Dr. D. Sebastián, Dr. A. S. Aricò, Dr. V. Baglio
Istituto di Tecnologie Avanzate per l'Energia "Nicola Giordano" (ITAE)
Consiglio Nazionale delle Ricerche (CNR)
Via Salita S. Lucia sopra Contesse 5, 98126, Messina (Italy)
E-mail: baglio@itae.cnr.it

[b] Dr. A. Serov, Dr. K. Artyushkova, Dr. J. Gordon, Prof. P. Atanassov
Department of Chemical and Biological Engineering and Center for Micro-Engineered Materials
Farris Engineering Center
University of New Mexico
Albuquerque, NM 87131 (USA)
E-mail: plamen@unm.edu

Supporting Information and the ORCID identification number(s) for the author(s) of this article can be found under <http://dx.doi.org/10.1002/cssc.201600583>.

emerging materials^[35] for alkaline DMFCs, have also been studied. In general, these catalysts are promising, especially M-N-C class, although further activity enhancement and especially electrode optimization is still needed.

We have recently reported outstanding performances of an iron aminoantipyrine derived catalyst at the cathode of a DMFC with a low PtRu content at the anode and high methanol molarity (30 mW cm⁻² with 10 M methanol).^[36] It appears that there is still room for further improvement on the basis of the cathode catalytic activity while maintaining a low PtRu content on the anode side. In the present work we investigate the influence of post-treatment of the synthesized aminobenzimidazole-derived M-N-C catalyst on the electrochemical performance of the fuel cells. It has been previously demonstrated that the treatment temperature, duration and ramp rate significantly influence the catalytic activity.^[37] The rationale herein has been to preliminary investigate the influence of heating and leaching treatments of the Fe-N-C catalysts on the ORR electrocatalytic activity in a rotating disk electrode (RDE) and rotating ring disk electrode (RRDE) configurations, as commonly reported in the literature.^[38–40] Thereafter, the most active formulation was further studied at the cathode of a DMFC under high energy density conditions (high methanol concentration) and cost-effectiveness (low PtRu loading at the anode). High methanol-tolerance together with a high density of active sites have resulted in a significant improvement of the DMFC performance with respect to the state of the art.

Results and Discussion

Fe-N_x-C (x=1–4) catalysts were prepared by the pyrolysis of iron nitrate mixed with aminobenzimidazole using a modified sacrificial support method (SSM) developed at the University of New Mexico (UNM). The catalytic activity towards the ORR was determined in acidic solution (0.5 M H₂SO₄) by the rotating disk electrode (RDE) technique, as depicted in Figure 1. Both PGM-free formulations show the typical sigmoidal wave, approaching a constant current density when scanning the potential to-

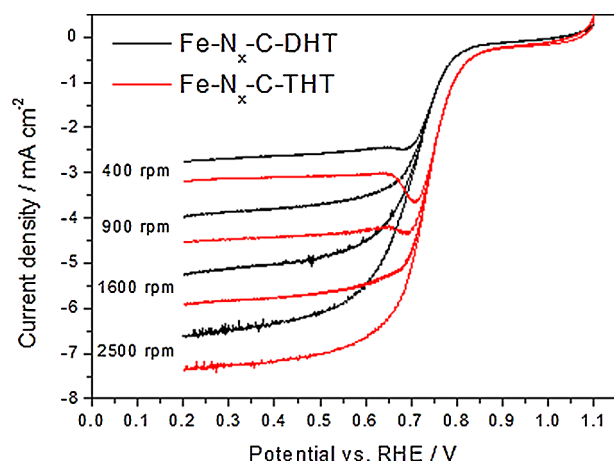


Figure 1. RDE curves for Fe-N_x-C-DHT (black) and Fe-N_x-C-THT (red) catalysts. O₂-saturated 0.5 M H₂SO₄, 5 mV s⁻¹, room temperature, 600 μg cm⁻² (not corrected for series resistance nor double-layer capacitance).

wards more negative values (i.e., higher overpotentials). Such a current density plateau is known as the diffusion limiting current and is shown by the Levich equation to depend on the square root of the rotation rate (ω) and the number of electrons involved in the reaction (n), for a given electrolyte. The difference in the limiting current density between a double heat-treated (Fe-N_x-C-DHT) and triple heat-treated (Fe-N_x-C-THT) catalyst at a fixed rotation rate indicates limiting diffusion constraints ascribed to the catalytic layer on the RDE (600 μg cm⁻²) as well as a small contribution from the higher Helmholtz double layer capacitance of the THT sample.

From a catalysis point of view, the difference in the kinetic-diffusion mixed region, that is, the intermediate region of the curves [0.5–0.9 V vs. the reversible hydrogen electrode (RHE)] is more interesting. The Fe-N_x-C-THT catalyst is clearly more active than the Fe-N_x-C-DHT catalyst, as indicated by the 35 mV shift. The enhancement of the ORR activity was attributed to substantial improvement of the synthetic methodology. The catalyst obtained after two heat-treatments (Fe-N_x-C-DHT) was subjected to additional leaching in 4 M HNO₃ to: a) remove iron nanoparticles covered with thin layers of graphitic carbon; b) remove amorphous carbon, which is prone to be corroded during the fuel cell operation; and c) expose the Fe-N_x active sites buried by the amorphous carbon layers. A third heat treatment (Fe-N_x-C-THT) in ammonia atmosphere was beneficial not only for cleaning of the surface from partially oxidized carbon-derived material, but also for creating additional Fe-N interactions. It should also decrease the oxygen content on the catalyst surface (NH₃ gas is a reducing agent at the treating temperature), which is beneficial for the increase of the catalyst hydrophobicity and for preventing the flooding of the pores by water and permeated methanol. At low rotation speed, a reduction peak appears at approximately 0.68–0.72 V versus RHE before achieving the diffusion limiting current, which is especially evident for the Fe-N_x-C-THT catalyst. This could be associated with the reduction of a redox couple (such as Fe²⁺/Fe³⁺) of the catalyst.^[41] However, the stable cyclic voltammograms in idle mode (Figure S1, Supporting Information) show only a small contribution of such a redox Fe²⁺/Fe³⁺ couple at approximately 0.4–0.65 V versus RHE, but with much lower current densities (< 0.2 mA cm⁻²). Therefore, it appears that the peak observed in the linear sweep voltammetry (LSV) at low ω shown in Figure 1 does not correspond with the reduction of the Fe²⁺/Fe³⁺. Thus, this reduction 'valley' at about 0.7 V versus RHE can be attributed to transient mass transport phenomena related to oxygen diffusivity in the catalytic layer, as reported for carbon-supported Pt catalysts.^[42] Thus, the use of a thick catalytic layer produces this 'valley' effect owing to oxygen concentration onto the catalyst surface higher than the oxygen saturation concentration in the electrolyte. This effect was further confirmed by using lower scan rates (Figure S2). The current related to the mentioned reduction 'valley' decreases if sweeping at 2 mV s⁻¹ and completely disappears at 0.5 mV s⁻¹, even with a low rotation speed (100 rpm).

Koutecky–Levich (K–L) plots obtained from RDE experiments are represented in Figure 2a. The K–L plots clearly show

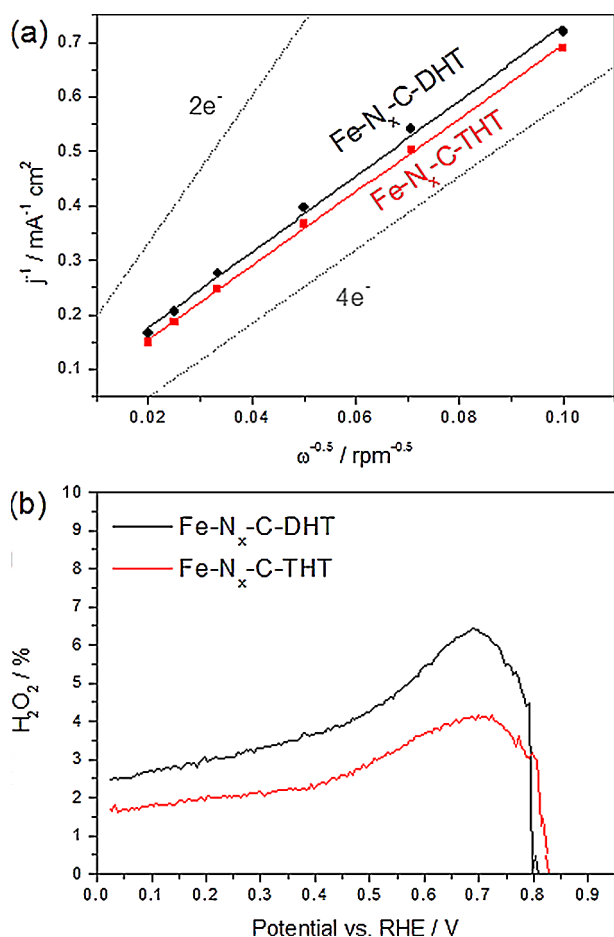


Figure 2. (a) Koutecký–Levich (0.5 V vs. RHE) in RDE configuration and (b) H_2O_2 yield in RRDE configuration, for $\text{Fe-N}_x\text{-C-DHT}$ and $\text{Fe-N}_x\text{-C-THT}$ catalysts in $0.5 \text{ M H}_2\text{SO}_4$, 1600 rpm , scan rate 5 mV s^{-1} , solution saturated with O_2 .

a linear behavior of the inverse of the current density (corrected by the double layer capacitance) with the reciprocal of the square root of the rotation speed. By applying the Levich equation to the linear fitting of the experimental data we calculated the transferred electron number (n) from the slope considering the O_2 concentration in saturated $0.5 \text{ M H}_2\text{SO}_4$ to be $1.26 \times 10^{-3} \text{ mol L}^{-1}$, the diffusion coefficient of molecular O_2 to be $1.93 \times 10^{-5} \text{ cm}^2 \text{ s}^{-1}$ and the kinetic viscosity of the electrolyte to be $0.01 \text{ cm}^2 \text{ s}^{-1}$.^[43,44] The n values calculated for the $\text{Fe-N}_x\text{-C-DHT}$ were in the range of $3.8\text{--}4.0$ and $3.9\text{--}4.0$ for the $\text{Fe-N}_x\text{-C-THT}$ catalyst in the same potential interval ($0.50\text{--}0.65 \text{ V vs. RHE}$), this is, in the mixed kinetic-diffusion-limited zone. Additional analysis of the number of electrons involved in the reaction was performed using the experimental data obtained using the RRDE configuration (Equation S1). The results show that n is approximately 3.9 in a broad potential range (from 0 to 0.6 V vs. RHE). The data from RRDE and K–L analysis are thus in perfect agreement, indicating that n is approximately 4 . An n value of approximately 4 indicates that an efficient mechanism in the electroreduction of oxygen to water proceeds through a $4e^-$ pathway. The difference between these two PGM-free catalysts is thus related to the kinetic current, as envisaged from the intercept of the fitted lines with the y -axis

of Figure 2a at a virtual $\omega^{-1/2} = 0$. The best kinetic currents are obtained for the $\text{Fe-N}_x\text{-C-THT}$ catalyst, which indicates a better ORR turnover frequency.

As described earlier, additional leaching with 4 M HNO_3 should result in the removal of carbon-covered iron nanoparticles. The Fe nanoparticles are well-known Fenton type radical producers and facilitate hydrogen peroxide generation. The latter process would affect the overall catalytic performance and durability (peroxide and radicals attack ionomers and membranes causing their degradation). RRDE studies were used to confirm the effectiveness of the removal of carbon-covered Fe nanoparticles. The calculation of the H_2O_2 yield was performed using Equation (1):

$$\% \text{H}_2\text{O}_2 = 100\% \frac{2j_r}{Nj_d + j_r} \quad (1)$$

where j_r is the current density on the ring, N is the collection efficiency of 40% , and j_d is the current density on the disk.

Figure 2b shows the H_2O_2 production (%) calculated by Equation (1) as a function of disk potential in the RRDE configuration. The variation of the H_2O_2 yield with potential is similar to previously published PGM-free catalysts.^[45] The $\text{Fe-N}_x\text{-C-THT}$ catalyst produces 40% less peroxide compared to $\text{Fe-N}_x\text{-C-DHT}$. Such a decrease in peroxide production is a direct indication of a partial shift of the ORR mechanism from a $2 \times 2e^-$ pathway, in which O_2 is first reduced to H_2O_2 followed by a second step of electroreduction of H_2O_2 to H_2O , to a direct $4e^-$ pathway of $\text{O}_2 \rightarrow \text{H}_2\text{O}$.^[46]

The differences in the catalytic behavior were also analyzed by Tafel plots, as shown in Figure 3. Very similar Tafel slopes of about 60 mV dec^{-1} were observed for both catalysts, which is a typical value also for Pt-based catalysts at low current densities.^[47] The difference between the $\text{Fe-N}_x\text{-C}$ catalysts is thus attributed to the exchange current density, j_0 , calculated as the intercept of the linear fittings with the x -axis at the equilibrium potential for ORR (1.23 V vs. RHE). The exchange current density is about two times higher for the THT catalyst compared

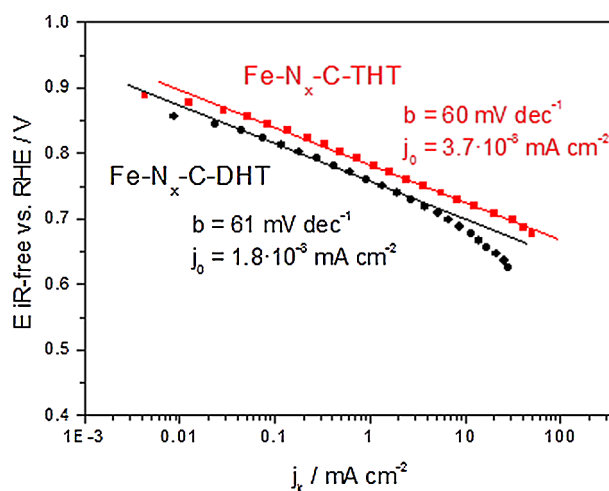


Figure 3. Tafel plots for the PGM-free formulations. O_2 -saturated $0.5 \text{ M H}_2\text{SO}_4$, room temperature, catalyst loading: $600 \mu\text{g cm}^{-2}$.

with the DHT catalyst. This is presumably related to a larger number of surface oxygen reduction active sites of the former, which are formed during the additional leaching and third heat treatment.

The physicochemical characterization of the Fe-N_x-C-THT catalyst was performed using microscopy techniques (SEM and TEM), N₂ physisorption (BET surface area) and surface chemical composition analysis by X-ray photoelectron spectroscopy (XPS). As shown in Figure 4, the Fe-N_x-C-THT catalyst is highly

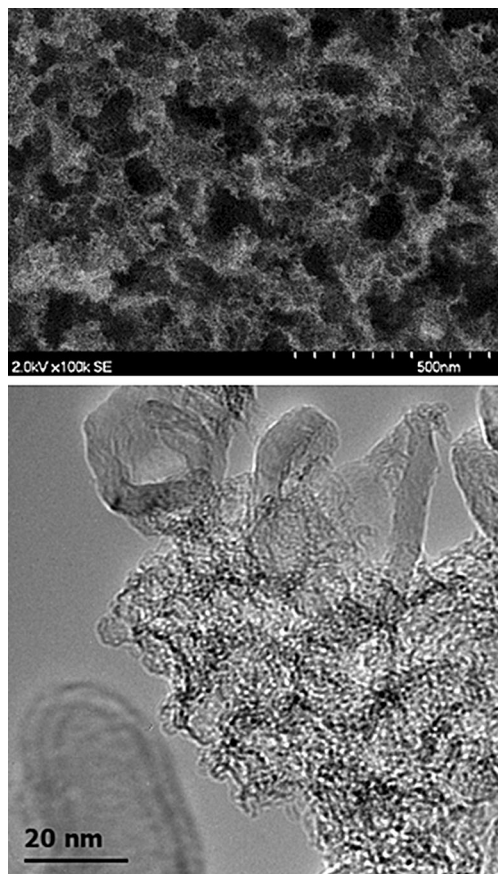


Figure 4. (a) SEM and (b) TEM images of the Fe-N_x-C-THT catalyst.

porous and exhibits the characteristic features of Fe-N-C catalysts made by SSM.^[48] Such a porous structure allows the ionomer to be integrated inside the catalyst layer, providing oxygen access to the active sites as well as allowing the removal of produced water. Notably, the leaching with 4 M HNO₃ resulted in the successful removal of iron nanoparticles covered with graphitic carbon layers (Figure 4b, top); the same phenomenon was observed and discussed in detail in a previously published work.^[49] The BET surface area was not changed after the second leaching and the third heat treatment and was similar to Fe-N_x-C-DHT, 620 m² g⁻¹.

High resolution XPS spectra were obtained to analyze the chemical species on the surface of the Fe-N_x-C catalysts (not shown). The elemental composition of the Fe-N_x-C-DHT and Fe-N_x-C-THT electrocatalysts was obtained using XPS data. The Fe-N_x-C-DHT sample has a significant amount of oxygen

Table 1. Chemical speciation of Fe-N_x-C-DHT and Fe-N_x-C-THT catalysts derived from XPS analysis survey spectra.

Sample	C 1s [%]	O 1s [%]	N 1s [%]	Fe 2p [%]
Fe-N _x -C-DHT	87.1	11.1	1.6	0.09
Fe-N _x -C-THT	91.2	5.5	3.1	0.13

(11.1%), which decreases to 5.5% after the third heat treatment (Table 1).

Interestingly, the Fe-N_x-C-THT sample has higher amounts of surface nitrogen and iron, which might increase the density of the active sites for ORR.^[46] The distribution of nitrogen and iron species is similar in both samples, so the overall chemistry of the Fe-N containing part of the electrocatalyst does not significantly change after additional leaching and the third heat treatment.^[49] Therefore, the removal of surface oxides, which is accompanied with the increase of hydrophobic carbon (graphitic C and C–C) as evidenced by carbon speciation analysis reported in Table 2, and the larger amount of atomic N and Fe present after the third heat treatment results in higher activity of the THT material.

Table 2. Carbon species distribution derived from C 1s deconvolution of the XPS spectra.

Sample	Graphitic C [%]	C–C [%]	C–N [%]	C _x O _y [%]
Fe-N _x -C-DHT	9.4	35.1	9.3	33.4
Fe-N _x -C-THT	12.5	38.9	10.8	29.1

For the application of DMFCs, it is highly desirable for the cathode catalyst to exhibit a high tolerance to the presence of methanol.^[50] Unreacted methanol permeates through the polymeric membrane in the membrane–electrode assembly (MEA) and reaches the cathode compartment. The adsorption of methanolic moieties on the surface of Pt (the benchmark cathode catalyst) causes a mixed potential, leading to a significant loss of cell efficiency. The tolerance to methanol poisoning of the Fe-N_x-C catalysts was studied in a half-cell configuration by adding methanol to the electrolyte solution and studying the ORR response. Figure 5 depicts the variation of the ORR half-wave potential ($E_{1/2}$)—that is, the potential at half the diffusion-limiting current density—with the increase of methanol concentration using a logarithmic scale. The complete set of curves are shown in Figure S2. For comparison, a commercial Pt/C (40 wt% Pt, Johnson Matthey) is included in the figure. Interestingly, the decrease of $E_{1/2}$ with increasing methanol concentration is only a few millivolts in both PGM-free catalysts, which is related to their extraordinarily high selectivity to the ORR.^[51] More specifically, the Fe-N_x-C-DHT and Fe-N_x-C-THT catalysts show only an 18 mV and 10 mV decay of $E_{1/2}$, respectively, when moving from 0.001 M to 1 M. In contrast, the Pt/C catalyst shows a sharp decrease of half-wave potential (about 200 mV) for concentrations higher than 0.01 M and then a smoother but not negligible shift towards more negative potentials,

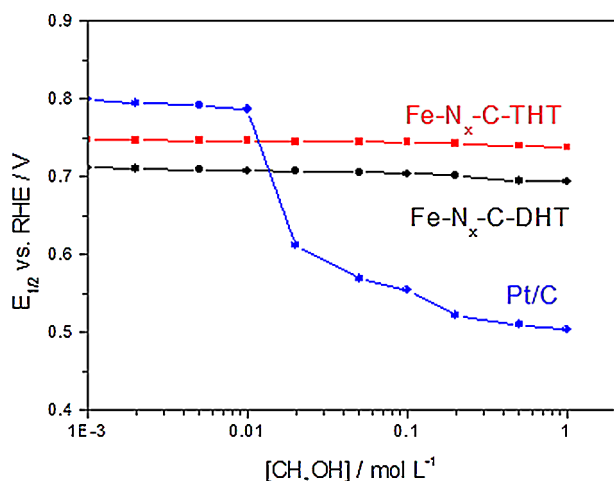


Figure 5. Methanol concentration effect on the half-wave ORR potential ($E_{1/2}$) in the O_2 -saturated $0.5\text{ M H}_2\text{SO}_4$ electrolyte, recorded by LSV at 1600 rpm and 5 mV s^{-1} , and comparison with Pt/C (40 wt% Pt, Johnson Matthey).

which results in a total $E_{1/2}$ decay of 296 mV in the same methanol concentration interval (from 0.001 to 1 M). A small part of the current decay with increasing methanol concentration is related to the change of the properties in the electrolyte solution with the addition of methanol, mainly oxygen saturation concentration and oxygen diffusivity. This would explain the $10\text{--}20\text{ mV}$ decay in the $\text{Fe-N}_x\text{-C}$ catalysts when moving from methanol-free to 1 M solution.

A performance analysis of the most active formulation, that is, the $\text{Fe-N}_x\text{-C-THT}$ catalyst, was performed in a single cell configuration DMFC. The PGM-free catalyst was studied at the cathode side of an MEA formed with a perfluorosulfonic acid (PFSA) membrane (Nafion[®] 115) and a commercial PtRu black catalyst (Johnson Matthey) at the anode side ($1\text{ mg}_{\text{PtRu}}\text{ cm}^{-2}$). The results obtained with this kind of analysis can be considered more realistic than those obtained in a half-cell configuration because of the occurrence of mass transport phenomena such as oxygen diffusivity, electrode flooding or permeated methanol local concentration, which are more complex to study in a three-electrode configuration; therefore, it offers a better indication of the performance of a DMFC in practical applications.

DMFC polarization and power density curves obtained at three different temperatures (30 , 60 and $90\text{ }^\circ\text{C}$) and four methanol concentrations (1 , 2 , 5 and 10 M) are shown in Figure 6. At low temperature ($30\text{--}60\text{ }^\circ\text{C}$) the maximum power density increases with methanol concentration. This may be attributed to improved methanol transfer at higher methanol concentrations, combined with the great tolerance of the $\text{Fe-N}_x\text{-C-THT}$ cathode to the permeated alcohol. Generally, Pt-cathode-based MEAs show a sharp decrease in performance when feeding with high methanol concentrations,^[36] whereby the detrimental crossover effect at the cathode is not compensated by the better performance of the anode. This is not the case of the MEA based on a $\text{Fe-N}_x\text{-C}$ cathode. The cell potential experiences mass transport constraints when feeding 1 M methanol, which is recovered by increasing the methanol molarity, as evi-

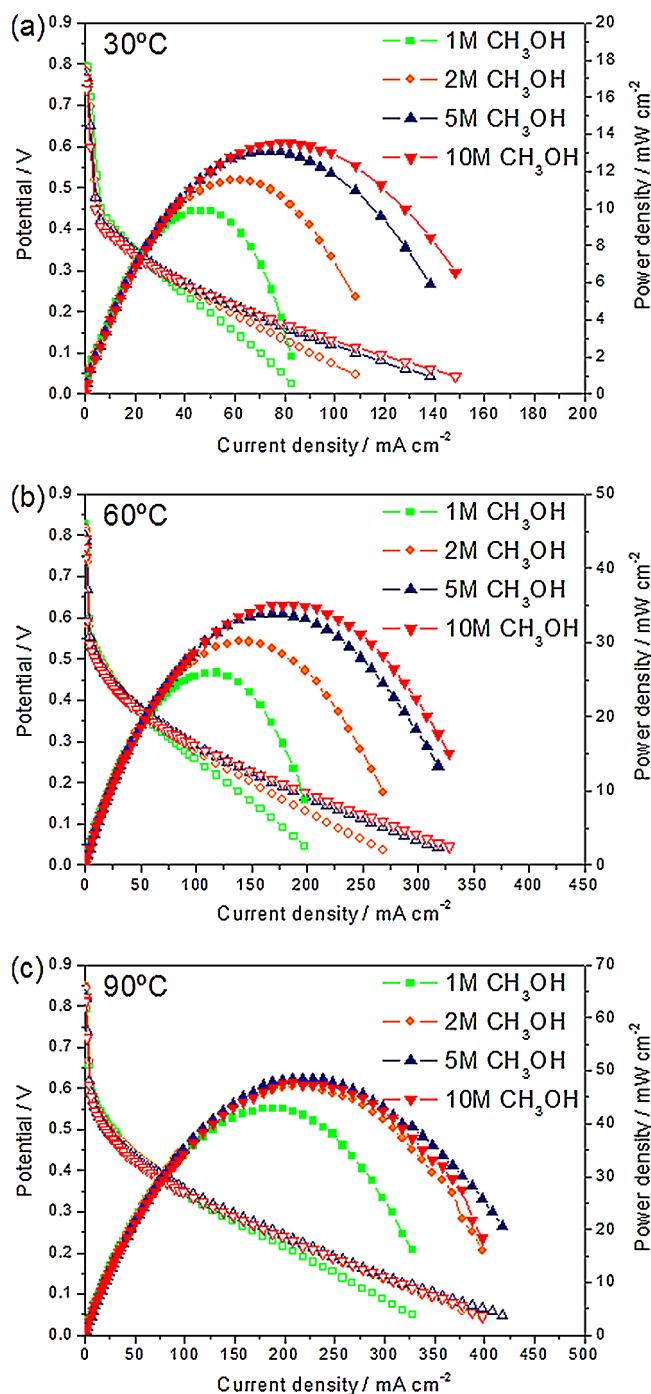


Figure 6. Influence of methanol molarity on DMFC polarization (empty symbols) and power density (filled symbols) curves at (a) $30\text{ }^\circ\text{C}$, (b) $60\text{ }^\circ\text{C}$ and (c) $90\text{ }^\circ\text{C}$ using the $\text{Fe-N}_x\text{-C-THT}$ catalyst at the cathode ($4.5 \pm 0.2\text{ mg cm}^{-2}$). Membrane: Nafion[®] 115. Anode: 1 mg PtRu cm^{-2} .

denced by the increase of cell potential at high current density.

Pure methanol contains 6100 mWh g^{-1} but the supply of water with the fuel is required for its oxidation (1 mol of water per mol of methanol), so aqueous solutions are generally employed. The energy density of a 10 M methanol solution is 2106 mWh g^{-1} whereas a 2 M solution contains only 393 mWh g^{-1} . Thus, a high methanol concentration is required

for the design of high energy density systems based on DMFCs. In the polarization curves shown in Figure 6a and 6b, it is remarkable that the cell potential does not vary with methanol concentration up to a certain current density value (30 mA cm^{-2} at 30°C or 60 mA cm^{-2} at 60°C). Indeed, the open circuit potential (OCP) barely changes, which is directly related to the methanol tolerance properties of the cathode. At high current densities, the differences observed owing to the variation of methanol concentration are related to the mass transport constraints at the anode side.

The polarization curves at 90°C show a slightly different behavior with methanol concentration, as shown in Figure 6c. In this case, there are no significant differences between the curves obtained with methanol molarities in the 2–10 M region. The cell potential is almost independent of methanol concentration from an OCP of 0.82–0.85 V up to approximately 0.3 V (135 mA cm^{-2}). At higher current densities only the curve related to the lowest methanol molarity (1 M) differs from the others and shows a lower performance. It appears that under high temperature and high methanol concentration conditions the overall cell performance is determined by the cathode rather than the anode. The maximum power density achieved is 48 mW cm^{-2} at 225 mA cm^{-2} and a cell potential of 0.22 V at a methanol feed concentration of 2–10 M to the anode side.

Figure 7 shows the variation of several cell operating parameters of interest in two working regimes, at different temperatures, and as a function of the methanol concentration. The comparison includes an MEA formed by a commercial Pt/C catalyst at the cathode (40 wt% Pt, Johnson Matthey) and identical configuration of the anode and membrane. In the activation controlled region (Figure 7a), most of the contribution to the cell behavior comes from the kinetic control of MOR and ORR. It is remarkable that in all cases the cell potential is higher for the PGM-free MEA (even at a low methanol concentration of 1 M). This indicates that, regardless of the temperature, the Fe-based catalyst is kinetically more active than the benchmark Pt-based catalyst. From the RDE half-cell characterization (Figure 5) it was deduced that this condition occurs only for local methanol concentrations above a certain value, at which the adsorption of the alcohol on the Pt active sites negatively affects the selectivity toward ORR, whereas the Fe-based catalyst still offers a high selectivity (virtually close to 100%). In this zone, that is, at low current density, the cell potential shows significantly different trends with methanol molarity depending on the cathode catalyst, Fe-N_x-C-THT or Pt/C. The PGM-free formulation almost maintains the cell potential with increasing methanol concentration, with a decay of only approximately 25 mV when moving from 1 to 10 M. This decay could be related to the oxygen transport variation at the cathode side derived from the presence of a higher methanol concentration. Instead, the MEA based on the Pt/C cathode exhibits a decay in the order of 100–170 mV under identical working conditions.

The performance analysis in the high power density region (0.2 V, Figure 7b) shows different trends than those derived from the activation controlled zone. In this case, the Fe-N-C-based MEA exhibits higher ($30^\circ, 90^\circ\text{C}$) or comparable (60°C)

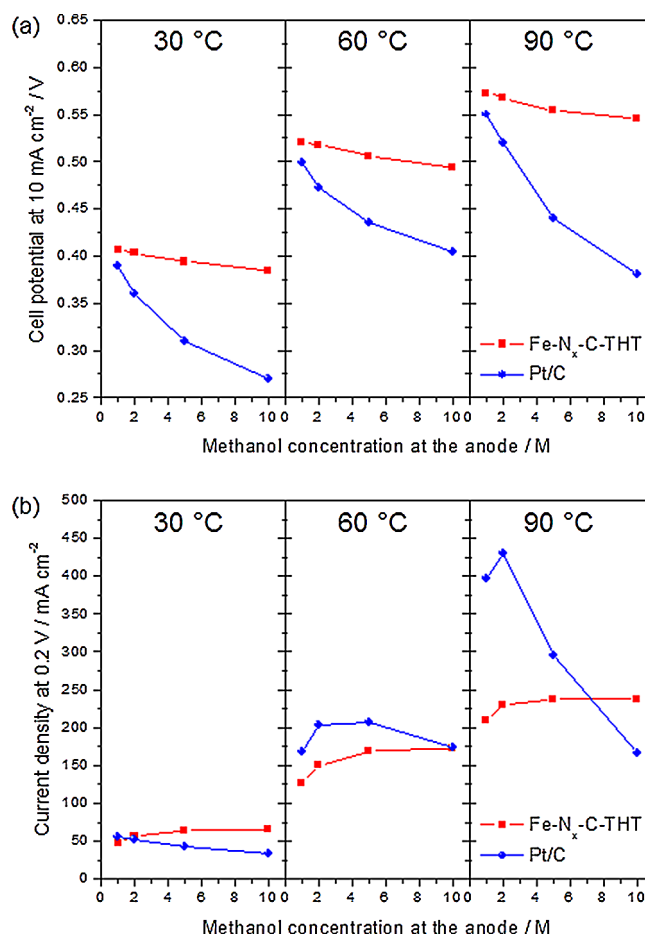


Figure 7. Effect of methanol concentration fed to the anode on (a) cell potential in the activation controlled region (10 mA cm^{-2}) and (b) current density at high power density regime (0.2 V). DMFCs are based on Fe-N_x-C-THT (red squares) and Pt/C (blue circles) cathodes. Three different operating temperatures ($30^\circ, 60^\circ$ and 90°C). Membrane: Nafion[®] 115. Anode: $1 \text{ mg}_{\text{PtRu}} \text{ cm}^{-2}$. Data of DMFC performance based on Pt/C cathode from ref. [36].

performances with respect to the Pt-based MEA when a high methanol concentration is used. At an intermediate–high temperature ($60\text{--}90^\circ\text{C}$) and methanol concentrations $\leq 5 \text{ M}$, the MEA based on the Pt/C cathode exhibits higher current densities. It is well-known that the methanol crossover effect decreases with current density.^[52] As a consequence, the gap between the PGM-free and the Pt formulations is reduced when operating in the high current density regime. The differences encountered may also be related to the different thicknesses of the catalytic layer; approximately $220\text{--}250 \mu\text{m}$ for the Fe-N_x-C-THT (4.5 mg cm^{-2}) and $70\text{--}90 \mu\text{m}$ for the Pt/C (1 mg Pt cm^{-2}). As a result, the average O₂ partial pressure is lower at the active sites of the Fe-N_x-C cathode owing to a higher pressure drop, leading to lower performance when demanding high current. This effect is not that evident at low temperature (30°C), at which the performance of the MEA based on the PGM-free cathode is higher. These results are promising for applications in low power devices working at near-ambient temperature such as small portable electronics.^[9] In summary, the Fe-N_x-C-THT catalyst investigated in this work outperforms Pt/C catalysts for application in high energy density DMFC systems

(> 10 M methanol molarity) and also under varying concentration at low temperature, such as air-breathing portable DMFCs. Moreover, the analysis of the kinetic behavior indicates that there is enormous potential to improve the performance by improving the electrode structure.

There have only been a few reports of the performance data of PGM-free catalysts at the cathode of DMFCs, presumably because of the relatively recent research interest in this topic. Figure 8 represent a summary of the latest reports of DMFC

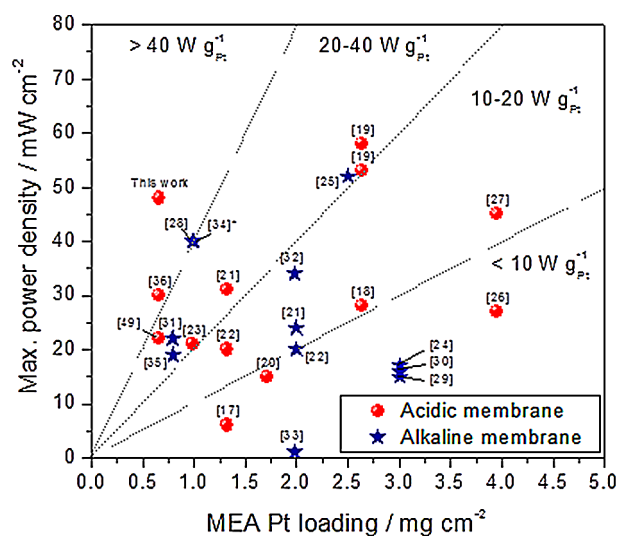


Figure 8. Latest DMFC performance results using acidic (red circles) or alkaline (blue stars) membrane and PGM-free catalysts at the cathode. For more details, please consult Table S1. *Pd (not Pt) was used at the anode side in Ref. [34]

performance using PGM-free formulations at the cathode. Further details (e.g., electrode composition, cell operating conditions) are provided in Table S1. The maximum power density is represented against the content of Pt in the MEA. Two MEA configurations have been differentiated according to the membrane: acidic (mostly PFSA-based membranes) and alkaline (mostly poly(arylene ether ketone) (PAEK)-based membranes). The major contribution to the total cost of the DMFC stack in such an MEA configuration is the Pt content of the anode and the polymeric membrane. At the anode side, PtRu and Pt catalysts are generally used in acidic and alkaline MEAs, respectively. Therefore, the PGM loading (mg cm^{-2}) at the anode has an important impact on the total cost of the MEA. In practice, moving towards the upper left side of the graph is mandatory to achieve low cost targets and maintain a high power density. In this regard, four regions have been identified in the figure in terms of specific power ($\text{W g}_{\text{Pt-MEA}}^{-1}$). It must be pointed out that the different cell operating conditions reported in the cited works lead to considerable differences in terms of power density, above all the cell temperature (most of them in the range 60–90 °C) and composition of the fuel/oxidant streams (most of them 2 M methanol and pure oxygen). The highest power density has been reported by Wei et al., achieving

58 mW cm^{-2} at 60 °C by using 10 mg cm^{-2} of an iron-based electrocatalyst combined with a N-doped carbon aerogel.^[19] They used $4 \text{ mg PtRu cm}^{-2}$ at the anode and Nafion® 117 as the polymeric membrane. Wan et al.^[34] reported a high performance of 40 mW cm^{-2} at 50 °C using a nitrogen-doped ordered mesoporous carbon at the cathode and a Pd catalyst at the anode with an alkaline membrane. It must be noted here that, in the latter work, the use of Pd represents an advantage since it has lower cost and larger abundance than Pt.^[53,54] Janarthanan et al.^[25] and Shen et al.^[28] have achieved good results using alkaline membranes operating at 80 °C, reaching 52 mW cm^{-2} with an Fe-N-C cathode and 40 mW cm^{-2} with a Co-N-C cathode, respectively. Our cost-effective acidic MEA shows the best results in terms of performance-to-cost ratio. Moreover, the Fe-N_x-C-THT cathode can be further optimized. Presumably, enhancing the electrode structure and optimizing the exposure of the active sites and diffusion of the reactants through the open porosity could lead to less mass transport losses at high current, and thus, improved performance.

Durability is also an important concern in the development of new DMFCs.^[55] Figure 9 shows a 100 h durability test at

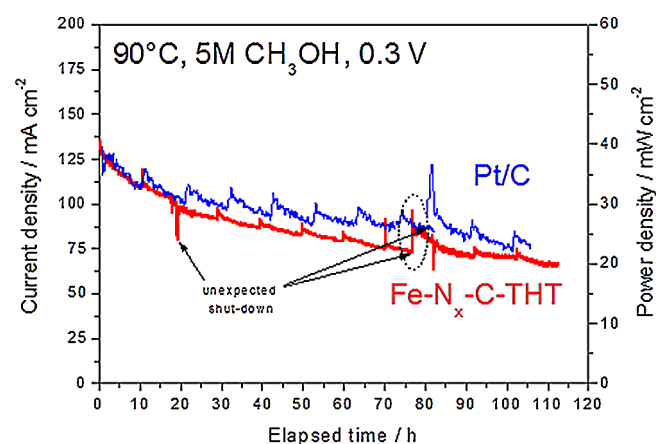


Figure 9. Stability test in DMFC at 0.3 V, 90 °C, 5 M CH₃OH fed to the anode and O₂ (100%RH) to the cathode. Anode 1 mg cm^{-2} PtRu black; membrane: Nafion® 115. Fe-N_x-C-THT cathode $4.5 \pm 0.2 \text{ mg cm}^{-2}$; Pt/C cathode $1.0 \pm 0.1 \text{ mg cm}^{-2}$.

0.3 V, 90 °C and 5 M methanol feed and fully humidified oxygen, performed on the MEA with Fe-N_x-C-THT catalyst at the cathode side. For comparison, a durability test performed under the same operating conditions is also shown for an MEA with Pt/C at the cathode side. A similar current–time (or power–time) behavior was registered for both MEAs. In the course of the experiments, unexpected shut-downs occurred as indicated in the figure, which may have slightly influenced the cell behavior. The performance variation with time is very similar between the two MEAs, accounting for about 50% steady-state performance decay in 100 h in the case of the Fe-N_x-C-THT cathode and about 45% in the case of the Pt/C cathode.

Conclusions

An aminobenzimidazole-derived iron PGM-free catalyst was physicochemically modified after synthesis by additional acid leaching and heat treatment steps. The activity towards the ORR was notably improved after the treatments, as evidenced in the half-cell experiments in acidic electrolyte. The physicochemical characterization, including XPS, BET, SEM, and TEM, indicated an increase of the density of Fe-N moieties as the cause of the improved catalytic activity. Experiments using rotating ring disk electrodes indicated a shift of the ORR mechanism from a $2 \times 2e^-$ to a $4e^-$ pathway as a consequence of the post-treatments of the Fe-N-C catalyst.

The treated catalyst also showed an exceptional tolerance to the presence of methanol. This was further investigated in a complete single cell fed with methanol, that is, a DMFC configuration, using the treated PGM-free catalyst at the cathode at a wide range of temperatures and methanol concentrations. The results indicated an outstanding performance, even at high methanol concentration (10 M), owing to improved ORR activity and high tolerance to the alcohol. Additionally, a 100 h experiment at high temperature showed a similar current-time behavior to a membrane-electrode assembly based on a benchmark Pt cathode. In summary, even with a relatively low PtRu content at the anode side, the presented results can be considered state-of-the-art for high-performance and cost-effective DMFCs.

Experimental Section

Synthesis and physicochemical characterization of Fe-N_x-C catalysts

A mixture of two types of commercial silica materials was used as a sacrificial support (LM150 with surface area of $150 \text{ m}^2 \text{ g}^{-1}$ and A90 with surface area of $90 \text{ m}^2 \text{ g}^{-1}$). Four grams of iron nitrate ($\text{Fe}(\text{NO}_3)_3 \cdot 9\text{H}_2\text{O}$, Sigma-Aldrich) was dissolved in 10 mL of acetone. In a separate beaker, 25 g of aminobenzimidazole (ABZIM) was dispersed in 100 mL of acetone. The blend of silica materials was added to a solution of ABZIM and a colloidal solution was obtained after ultrasonic treatment for 4 h in a low energy ultrasonic bath. Iron nitrate solution was added to the $\text{SiO}_2/\text{ABZIM}$ suspension under vigorous stirring. Acetone was evaporated and the mixture was ball-milled in a planetary ball mill at 400 rpm for 2 h. The finely homogenized mixture of precursors was heat treated in an inert atmosphere of ultrahigh purity (UHP) nitrogen at a flow rate of 150 mL min^{-1} at 945°C for 60 min. The mixture of silica was removed by means of 25 wt% of HF for 7 days. The powder was washed with deionized water until neutral pH was achieved. To remove the low soluble but volatile silica compounds, a second treatment in ammonia atmosphere (10% of NH_3) was performed at 975°C for 45 min. The obtained material was denoted as Fe-N_x-C-DHT (DHT: double heat treated). An additional treatment with 4 M HNO_3 was performed at room temperature for 48 h to remove iron nanoparticles coated with a graphitic layer (centers for Fenton type radical production). The remaining HNO_3 material was washed and heat treated a third time in an atmosphere of 7 at% NH_3 at 975°C for 15 min. The as obtained catalyst was used in the present study and denoted as Fe-N_x-C-THT (THT: triple heat treated). This latter catalyst was physicochemically characterized. SEM and TEM

images were obtained using Hitachi S-800 and JEOL 2010 EX instruments, respectively. The surface areas were measured by N_2 adsorption BET using a Micrometrics 2360 Gemini Analyzer. A four-point BET analysis was performed using a saturation pressure of 640 mmHg. The X-ray photoelectron spectroscopy (XPS) spectra were acquired on a Kratos Axis DLD Ultra X-ray photoelectron spectrometer using a monochromatic AlK_{α} source operating at 150 W with no charge compensation. The base pressure was 2×10^{-10} Torr, and the operating pressure was approximately 2×10^{-9} Torr. Survey and high-resolution spectra were acquired at pass energies of 80 and 20 eV, respectively. Data analysis and quantification were performed using CasaXPS software. A linear background subtraction was used for the quantification of the spectra. Sensitivity factors provided by the manufacturer were utilized. A 70% Gaussian/30% Lorentzian line shape was utilized in the curve-fit of the high resolution spectra.

Electrochemical characterization (RDE and RRDE)

The electrochemical characterization was performed in a three-electrode cell at room temperature for the PGM-free catalysts (Fe-N_x-C-DHT and Fe-N_x-C-THT) and a benchmark Pt/C catalyst (40 wt% Pt, Johnson Matthey) for comparison purposes. For the activity analyses, a rotating disk electrode (RDE) was used as the working electrode, consisting of a thin film of the catalyst deposited on a glassy carbon disk (geometric area of 0.196 cm^2). The H_2O_2 yield was determined using a rotating ring disk electrode (RRDE) consisting of a glassy carbon disk (geometric area of 0.247 cm^2) and a platinum ring. The catalytic layer was obtained using the following recipe: first, we prepared a 3 mg mL^{-1} ink by sonicating the catalyst in isopropyl alcohol/water (3/1, v/v) solution and Nafion® (Ion Power, 5 wt%) using an appropriate catalyst-to-ionomer ratio. Some drops of this ink were deposited onto the glassy carbon disk up to the desired mass loading for an optimum characterization:^{56,57} $600 \mu\text{g cm}^{-2}$ and 15 wt% Nafion®. An aqueous 0.5 M H_2SO_4 solution was used as an electrolyte, the reference electrode was a mercury/mercury sulfate electrode ($\text{Hg}|\text{Hg}_2\text{SO}_4$, sat. K_2SO_4) and a high surface Pt coiled wire was used as counter electrode. Tests performed using a high surface area graphite rod confirmed that the ORR curves were identical regardless of the counter electrode (Figure S4), which excluded any effect of eventual Pt redeposition from the counter electrode on the ORR electrocatalytic activity of the PGM-free catalysts. An Autolab potentiostat/galvanostat was used to perform the RDE electrochemical experiments. A Pine Instruments bipotentiostat was used for the RRDE experiments, using 1.5 V versus RHE as the ring potential. Linear sweep voltammetry curves were obtained in the potentiostatic mode with a scan rate of 5 mV s^{-1} and at rotation rates from 100–2500 rpm. The tolerance of the catalysts to the presence of methanol was evaluated in RDE by adding increasing aliquots of the alcohol to the base electrolyte, saturated with oxygen, at concentrations of 0.001–2 M. The ORR response in the presence of methanol was evaluated at a rotation speed of 1600 rpm.

Fuel cell testing (DMFC)

For single cell experiments, MEAs were prepared with the PGM-free Fe-N_x-C-THT catalyst at the cathode side. Cathode electrodes were obtained by spraying a catalytic ink on a commercial hydrophobic gas diffusion layer (GDL-LT, E-TEK). The catalyst ink was prepared by sonicating the catalyst in an isopropyl alcohol/water mixture (3/1, v/v) and Nafion® solution. The cathode electrode loading for the Fe-N_x-C-THT was $4.5 \pm 0.2 \text{ mg cm}^{-2}$ and the Nafion® content

in the catalytic layer was 45 wt%.^[58] Anode electrodes based on PtRu black (Pt:Ru 1:1, Johnson Matthey) were prepared according to the procedure described in a previous report.^[59] The catalytic layer was composed of 85 wt% catalyst and 15 wt% Nafion[®] ion-omer spread onto a commercial gas diffusion layer (GDL-HT, E-TEK). The noble metal (Pt+Ru) loading at the anode was 1 mg cm⁻².

MEAs were assembled by a hot-pressing procedure at 130 °C and 30 kgf cm⁻² for 10 min, and subsequently installed in a 5 cm² fuel cell test fixture (Fuel Cell Tech., Inc.). A Nafion[®] 115 membrane (≈ 130 μm thick) was used as the solid electrolyte; the anode loading was 1 mg PtRu cm⁻² (PtRu black, Johnson Matthey) for all the MEAs. The cell hardware was connected to a Fuel Cell Tech., Inc. test station. In case of single cell polarization experiments, aqueous methanol (1–10 M) was pre-heated at the same temperature of the cell and fed to the anode chamber of the DMFC through a peristaltic pump; oxygen was also pre-heated at the same temperature of the cell (fully humidified) and fed to the cathode side. The reactant flow rates were 2 and 100 mL min⁻¹ for the methanol/water mixture and oxygen streams, respectively. The cell temperature was measured by a thermocouple embedded in the cathodic graphite plate close to the MEA. Steady-state galvanostatic polarization experiments in DMFC were performed with an Agilent electronic load at various temperatures and methanol concentrations.

Acknowledgements

CNR-ITAE authors acknowledge the financial support of PRIN2010-11 project 'Advanced nanocomposite membranes and innovative electrocatalysts for durable polymer electrolyte membrane fuel cells' (NAMED-PEM).

Keywords: direct methanol fuel cell • electrocatalyst • methanol tolerance • oxygen reduction reaction • post-treatment

- A. S. Aricò, P. Bruce, B. Scrosati, J.-M. Tarascon, W. van Schalkwijk, *Nat. Mater.* **2005**, *4*, 366–377.
- N. Radenahmad, A. Afif, P. I. Petra, S. M. H. Rahman, S.-G. Eriksson, A. K. Azad, *Renewable Sustainable Energy Rev.* **2016**, *57*, 1347–1358.
- Y. Chen, M. Bellini, M. Bevilacqua, P. Fornasiero, A. Lavacchi, H. A. Miller, L. Wang, F. Vizza, *ChemSusChem* **2015**, *8*, 524–533.
- S. K. Kamarudin, F. Achmad, W. R. W. Daud, *Int. J. Hydrogen Energy* **2009**, *34*, 6902–6916.
- P. Joghee, J. N. Malik, S. Pylypenko, R. O'Hayre, *MRS Energy Sustainable* **2015**, *2*, E3.
- J. Han, H. Liu, *J. Power Sources* **2007**, *164*, 166–173.
- C. Y. Du, T. S. Zhao, W. W. Yang, *Electrochim. Acta* **2007**, *52*, 5266–5271.
- B. Gurau, E. S. Smotkin, *J. Power Sources* **2002**, *112*, 339–352.
- D. S. Falcão, V. B. Oliveira, C. M. Rangel, A. M. F. R. Pinto, *Renewable Sustainable Energy Rev.* **2014**, *34*, 58–70.
- L. Li, S. Liu, A. Manthiram, *Nano Energy* **2015**, *12*, 852–860.
- S. Liu, L. Li, H. S. Ahn, A. Manthiram, *J. Mater. Chem. A* **2015**, *3*, 11615–11623.
- M. Jahan, Q. Bao, K. P. Loh, *J. Am. Chem. Soc.* **2012**, *134*, 6707–6713.
- N. A. Karim, S. K. Kamarudin, *Appl. Energy* **2013**, *103*, 212–220.
- G. Wu, A. Santandreu, W. Kellogg, S. Gupta, O. Ogoke, H. Zhang, H.-L. Wang, L. Dai, *Nano Energy* **2016**, DOI: 10.1016/j.nanoen.2015.12.032.
- S. Chen, D. Higgins, A. Yu, L. Zhang, J. Zhang, *Energy Environ. Sci.* **2011**, *4*, 3167.
- F. Jaouen, E. Proietti, M. Lefèvre, R. Chenitz, J.-P. Dodelet, G. Wu, H. T. Chung, C. M. Johnston, P. Zelenay, *Energy Environ. Sci.* **2011**, *4*, 114–130.
- S. Baranton, C. Coutanceau, J.-M. Léger, C. Roux, P. Capron, *Electrochim. Acta* **2005**, *51*, 517–525.
- A. A. Serov, M. Min, G. Chai, S. Han, S. J. Seo, Y. Park, H. Kim, C. Kwak, *J. Appl. Electrochem.* **2009**, *39*, 1509–1516.
- Y. Wei, C. Shengzhou, L. Weiming, *Int. J. Hydrogen Energy* **2012**, *37*, 942–945.
- E. Negro, A. H. A. M. Videla, V. Baglio, A. S. Aricò, S. Specchia, G. J. M. Koper, *Appl. Catal. B* **2015**, *166–167*, 75–83.
- J. Zhu, M. Xiao, C. Liu, J. Ge, J. St-Pierre, W. Xing, *J. Mater. Chem. A* **2015**, *3*, 21451–21459.
- M. Xiao, J. Zhu, L. Feng, C. Liu, W. Xing, *Adv. Mater.* **2015**, *27*, 2521–2527.
- Y. Hu, J. Zhu, Q. Lv, C. Liu, Q. Li, W. Xing, *Electrochim. Acta* **2015**, *155*, 335–340.
- J. Liu, X. Sun, P. Song, Y. Zhang, W. Xing, W. Xu, *Adv. Mater.* **2013**, *25*, 6879–6883.
- R. Janarthanan, A. Serov, S. K. Pilli, D. A. Gamarra, P. Atanassov, M. R. Hibbs, A. M. Herring, *Electrochim. Acta* **2015**, *175*, 202–208.
- T. S. Olson, B. Blizanac, B. Piela, J. R. Davey, P. Zelenay, P. Atanassov, *Fuel Cells* **2009**, *9*, 547–553.
- B. Piela, T. S. Olson, P. Atanassov, P. Zelenay, *Electrochim. Acta* **2010**, *55*, 7615–7621.
- M. Shen, L.-R. Zheng, W. He, C. Ruan, C. Jiang, K. Ai, L. Lu, *Nano Energy* **2015**, *17*, 120–130.
- X. Sun, P. Song, Y. Zhang, C. Liu, W. Xu, W. Xing, *Sci. Rep.* **2013**, *3*, 2505.
- X. Sun, Y. Zhang, P. Song, J. Pan, L. Zhuang, W. Xu, W. Xing, *ACS Catal.* **2013**, *3*, 1726–1729.
- S. Zhao, H. Yin, L. Du, L. He, K. Zhao, L. Chang, G. Yin, H. Zhao, S. Liu, Z. Tang, *ACS Nano* **2014**, *8*, 12660–12668.
- H. Zhong, J. Wang, Y. Zhang, W. Xu, W. Xing, D. Xu, Y. Zhang, X. Zhang, *Angew. Chem. Int. Ed.* **2014**, *53*, 14235–14239; *Angew. Chem.* **2014**, *126*, 14459–14463.
- I. Kruusenberg, S. Ratso, M. Vikkisk, P. Kanninen, T. Kallio, A. M. Kannan, K. Tammeveski, *J. Power Sources* **2015**, *281*, 94–102.
- K. Wan, G.-F. Long, M.-Y. Liu, L. Du, Z.-X. Liang, P. Tsiakaras, *Appl. Catal. B* **2015**, *165*, 566–571.
- M. Lei, J. Wang, J. R. Li, Y. G. Wang, H. L. Tang, W. J. Wang, *Sci. Rep.* **2014**, *4*, 6013.
- D. Sebastián, V. Baglio, A. S. Aricò, A. Serov, P. Atanassov, *Appl. Catal. B* **2016**, *182*, 297–305.
- A. Serov, M. H. Robson, B. Halevi, K. Artyushkova, P. Atanassov, *Electrochim. Commun.* **2012**, *22*, 53–56.
- F. Jaouen, V. Goellner, M. Lefèvre, J. Herranz, E. Proietti, J. P. Dodelet, *Electrochim. Acta* **2013**, *87*, 619–628.
- G. C.-K. Liu, J. R. Dahn, *Appl. Catal. A* **2008**, *347*, 43–49.
- K. Wan, Z. Yu, X. Li, M. Liu, G. Yang, J. Piao, Z. Liang, *ACS Catal.* **2015**, *5*, 4325–4332.
- U. Tylus, Q. Jia, K. Strickland, N. Ramaswamy, A. Serov, P. Atanassov, S. Mukerjee, *J. Phys. Chem. C* **2014**, *118*, 8999–9008.
- J. Jiang, B. Yi, *J. Electroanal. Chem.* **2005**, *577*, 107–115.
- N. M. Markovic, H. A. Gasteiger, P. N. Ross, *J. Phys. Chem.* **1995**, *99*, 3411–3415.
- V. Stamenkovic, N. M. Markovic, P. N. Ross, *J. Electroanal. Chem.* **2001**, *500*, 44–51.
- M. H. Robson, A. Serov, K. Artyushkova, P. Atanassov, *Electrochim. Acta* **2013**, *90*, 656–665.
- K. Artyushkova, A. Serov, S. Rojas-Carbonell, P. Atanassov, *J. Phys. Chem. C* **2015**, *119*, 25917–25928.
- D. B. Sepa, M. V. Vojnovic, A. Damjanovic, *Electrochim. Acta* **1981**, *26*, 781–793.
- A. Serov, K. Artyushkova, N. I. Andersen, S. Stariha, P. Atanassov, *Electrochim. Acta* **2015**, *179*, 154–160.
- D. Sebastián, A. Serov, K. Artyushkova, P. Atanassov, A. S. Aricò, V. Baglio, *J. Power Sources* **2016**, *319*, 235–246.
- E. Antolini, T. Lopes, E. R. Gonzalez, *J. Alloys Compd.* **2008**, *461*, 253–262.
- T. S. Olson, S. Pylypenko, S. Kattel, P. Atanassov, B. Kiefer, *J. Phys. Chem. C* **2010**, *114*, 15190–15195.
- A. S. Arico, V. Baglio, V. Antonucci, *Direct Methanol Fuel Cells*, Nova Science Publishers, Inc., **2010**.
- A. S. Aricò, A. Stassi, C. D'Urso, D. Sebastián, V. Baglio, *Chem. Eur. J.* **2014**, *20*, 10679–10684.

- [54] R. Carrera-Cerritos, V. Baglio, A. S. Aricò, J. Ledesma-García, M. F. Sgroi, D. Pullini, A. J. Pruna, D. B. Mataix, R. Fuentes-Ramírez, L. G. Arriaga, *Appl. Catal. B* **2014**, *144*, 554–560.
- [55] A. Mehmood, M. A. Scibioh, J. Prabhuram, M.-G. An, H. Y. Ha, *J. Power Sources* **2015**, *297*, 224–241.
- [56] A. Serov, U. Tylus, K. Artyushkova, S. Mukerjee, P. Atanassov, *Appl. Catal. B* **2014**, *150–151*, 179–186.
- [57] A. Bonakdarpour, M. Lefevre, R. Yang, F. Jaouen, T. Dahn, J.-P. Dodelet, J. R. Dahn, *Electrochem. Solid-State Lett.* **2008**, *11*, B105.
- [58] A. Serov, K. Artyushkova, P. Atanassov, *Adv. Energy Mater.* **2014**, *4*, 1301735.
- [59] V. Baglio, C. D'Urso, D. Sebastián, A. Stassi, A. S. Aricò, *Int. J. Hydrogen Energy* **2014**, *39*, 5399–5405.

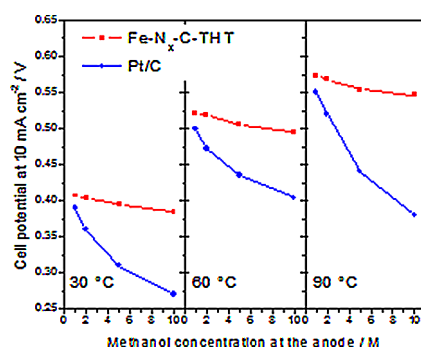
Received: May 2, 2016

Revised: May 20, 2016

Published online on ■ ■ ■■, 0000

FULL PAPERS

No nobles here! Platinum group metal-free materials based on Fe-N-C are investigated as cost-effective, active, stable and methanol-tolerant catalysts for the oxygen reduction reaction (ORR) in direct methanol fuel cells (DMFCs). Outstanding performance of DMFCs is observed, even at high methanol concentration (10 M), owing to improved ORR activity and high tolerance to the alcohol.



D. Sebastián, A. Serov, K. Artyushkova, J. Gordon, P. Atanassov, A. S. Aricò, V. Baglio**



High Performance and Cost-Effective Direct Methanol Fuel Cells: Fe-N-C Methanol-Tolerant Oxygen Reduction Reaction Catalysts

